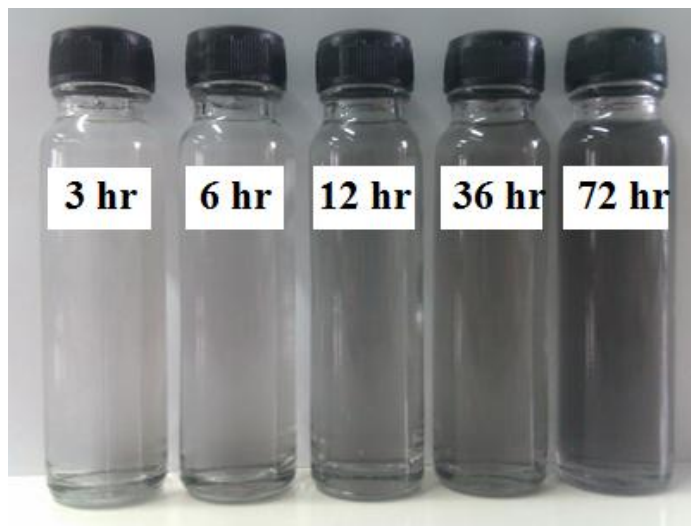


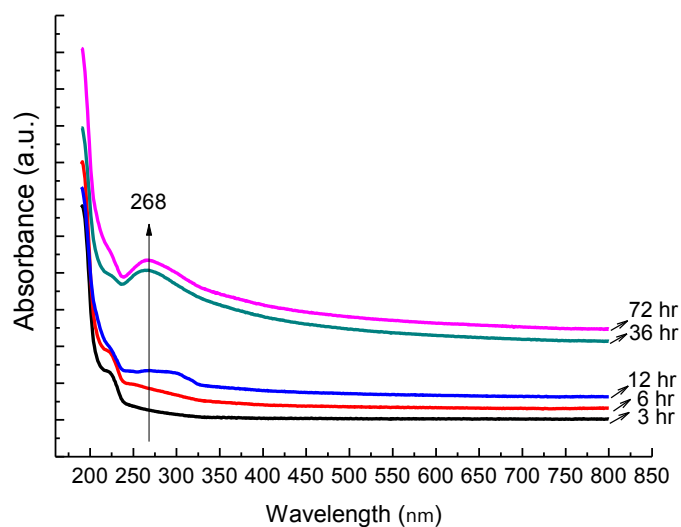
## CHAPTER 4 RESULTS AND DISCUSSION

### 4.1 Nanographite

Figure 4.1 showed picture of nanographite dispersions prepared from 6, 12, 36, and 72 hours of sonication. The color of the dispersions became darker for longer time of sonication because it enhanced the concentration of nanographite in the dispersion. Sonication time also affected the homogeneity and sedimentation of the nanographite suspensions. The suspension from the sonication times of 36 and 72 hours stayed stable, e.g. without aggregation, for more than 3 months.

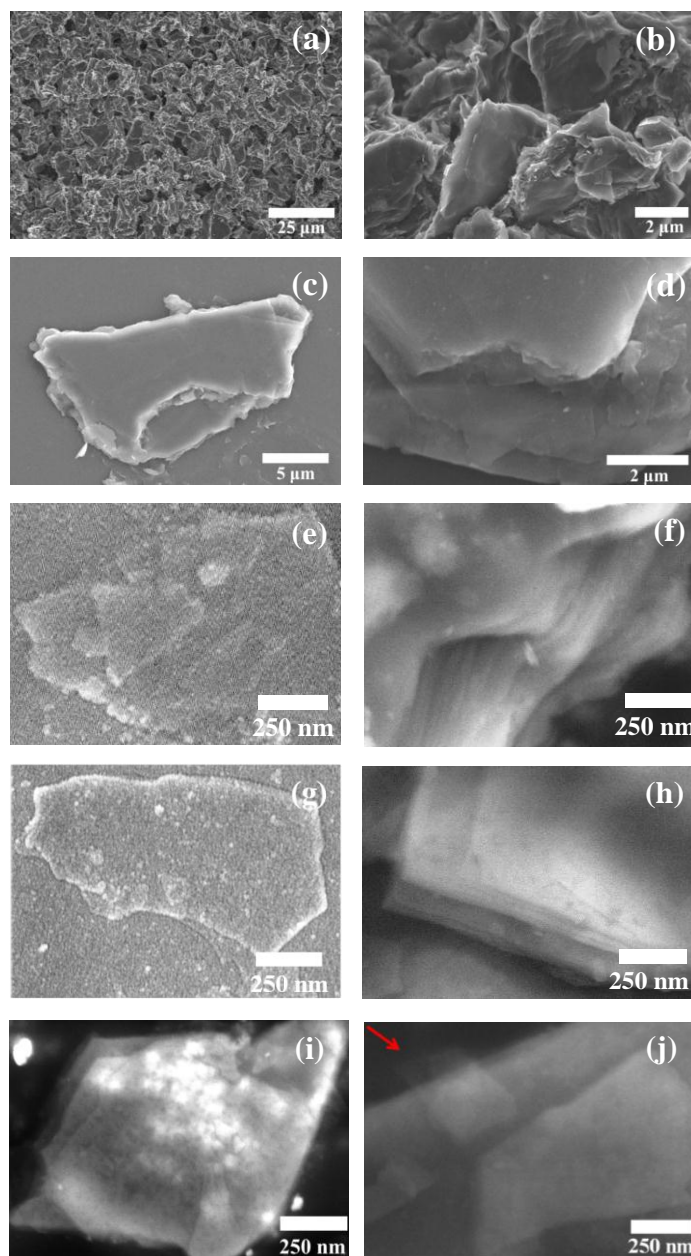


**Figure 4.1** Photograph of nanographite suspensions prepared from different times of sonication, including 3, 6, 12, 36, and 72 hours



**Figure 4.2** UV-Vis absorption spectra of nanographite suspensions prepared from different times of sonication, including 3, 6, 12, 36, and 72 hours

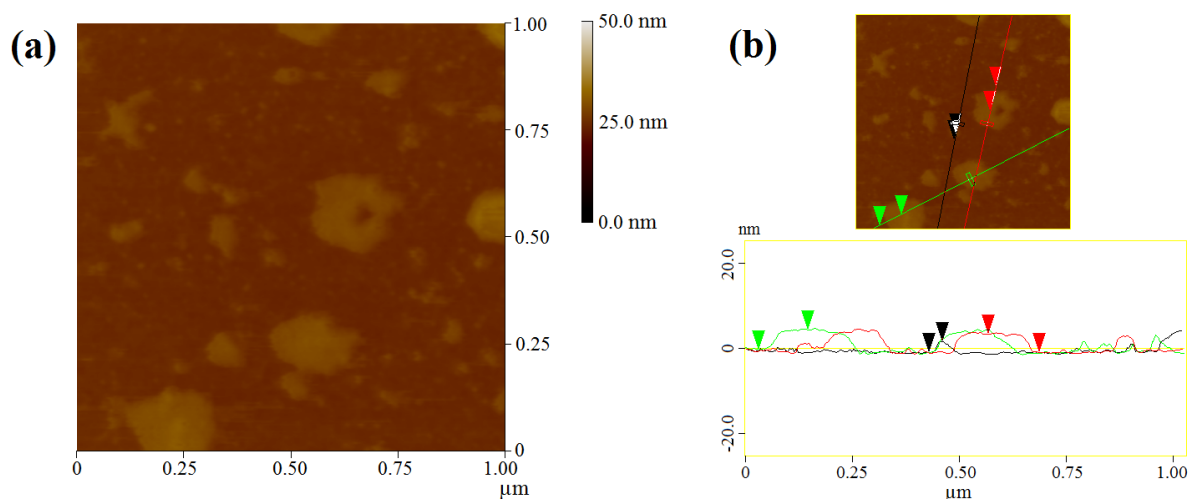
Figure 4.2 showed UV-Vis absorption spectra for nanographite suspensions prepared from different sonication times: 3, 6, 12, 36, and 72 hours. The absorption peak of the nanographite suspensions at 268 nm gradually increased from 3 hours to 72 hours of sonication. This result indicated that there were some changes in the concentration of nanographite in the dispersion, i.e. longer time of sonication broke nanographite from its parent graphite. The absorption of UV or visible light in this region is due to the electronic transitions between the  $\pi \rightarrow \pi^*$  transitions of the C=C nature [54]. The spectra confirmed that nanographite could be able to disperse in distilled water.



**Figure 4.3** SEM images of nanographite obtained from different times of sonication. (a) – (b) raw graphite, (c) – (d) 3 hours of sonication, (e) – (f) 6 hours of sonication, (g) – (h) 36 hours of sonication and (i) – (j) 72 hours of sonication

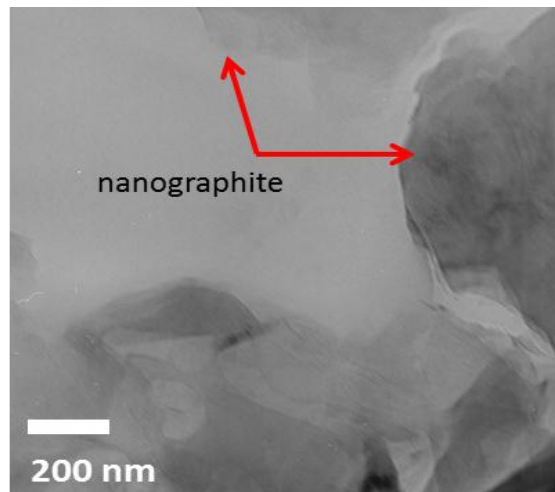
Figure 4.3 showed SEM images of raw graphite and nanographite obtained from different times of sonication. The exfoliation processes began after 3 hours of sonication, where the small part of graphite came out of the bulk graphite as shown in figure 4.3(c) and (d). The thickness of the graphite was about 2 - 4  $\mu\text{m}$ , implying that there were plenty of graphene stacked on the graphite. At 6 hours of sonication, the graphite flake became thinner and its thickness was about 300 – 800 nm as shown in figure 4.3(e) and (f). Longer time of sonication significantly decreased the thickness of the graphite. At 36 hour of sonication, the thickness of the graphite flake was almost less than 250 nm. At 72 hour of sonication, the thickness of the graphite flake was less 100 nm. Thus, we could call this sample ‘nanographite’ as it met the definition of nanomaterial. As shown in figure 4.3(j), the red arrow pointed to the nanographene or even multilayer graphene.

Figure 4.4 showed AFM images of nanographite which obtained from 72 hours of sonication with its height profile. AFM height profile indicated that bulk graphite was almost completely exfoliated and became nanographite suspended in distilled water. Height profile in figure 4.4 indicated that the thickness of nanographite is less than 5 nm. The calculated result implied that most of them were less than 15 layers of single layer graphene.



**Figure 4.4** (a) AFM height image of nanographite obtained from 72 hours of sonication (b) Height profile for the sheets marked by the green, black and red lines in figure (a)

Figure 4.5 showed TEM image of nanographite prepared from sonication technique. It confirmed that sonication has a positive effect on nanographite exfoliation. This figure implied that there are plenty of graphene stacked on the graphite which may correspond to SEM and AFM images.



**Figure 4.5** TEM image of nanographite prepared from sonication technique

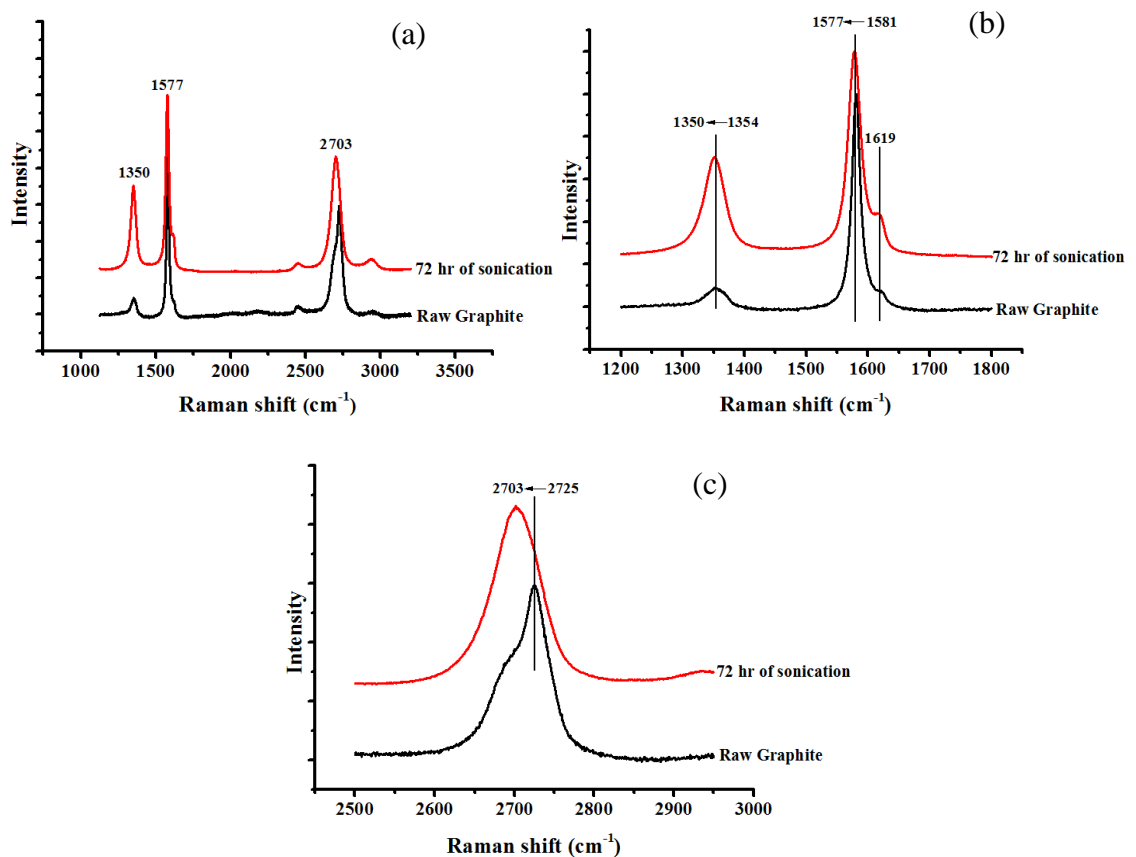


**Figure 4.6** (a) Raman spectra of raw graphite and nanographite (72 hours of sonication) (b) D and G bands (c) 2D bands

Figure 4.6 showed Raman spectra of raw graphite and nanographite (72 hours of sonication). The G-band is at about  $1577\text{--}1581\text{ cm}^{-1}$  which is from the stretching vibration of any pair of  $sp^2$  sites, whether in  $C=C$  chains. The D band is at about  $1350\text{--}1354\text{ cm}^{-1}$  which is the breathing mode of those  $sp^2$  sites only in rings, not in chains [55]. Nevertheless, the conversion of hybridization from a  $sp^2$  hybridized carbon to be a

$sp^3$  hybridized carbon caused a change in the Raman shift and an increase in the intensity of D band. D band generally involves the resonantly enhanced scattering of an electron via phonon emission by a defect which breaks the fundamental symmetry of the graphene sheet [56, 57]. The increase of the peak intensity in the D band of nanographite (72 hour sonication) may come from the increasing of the  $sp^3$  atom and the disordered structure of graphite. For example, 72 hours of sonication generated many nanographite. Moreover, Raman spectra of nanographite at  $1619\text{ cm}^{-1}$  may attribute to disordered carbon black, glassy carbon, nanographite [58]. The 2D band peak of raw graphite that was changed in the Raman position from  $2725\text{ cm}^{-1}$  to  $2703\text{ cm}^{-1}$  after 72 hour of sonication may correspond to the exfoliation of nanographite which was in agreement with the AFM images.

The crystallite size of nanographite that may attribute the plane size of nanographite is about 32.49 nm, which is obtained by Raman experiment using calculating by Eq. (4.1) [59].

$$L_a(\text{nm}) = \frac{560}{E_1^4} \left( \frac{I_D}{I_G} \right)^{-1} \quad (4.1)$$

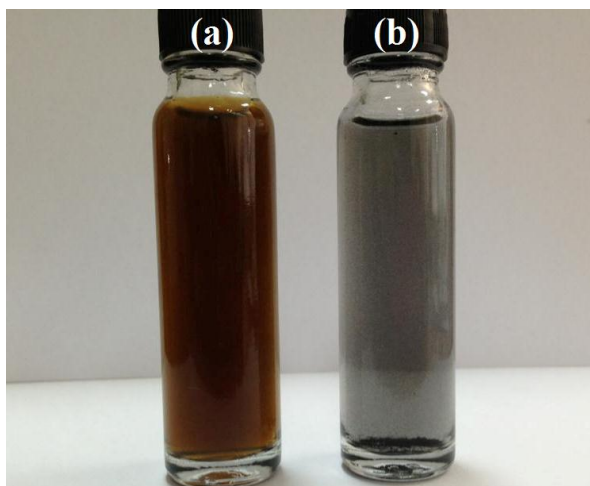
where  $I_D/I_G$  is the intensity ratio of the D and G bands.  $E_1$  is the excitation laser energy in eV units. Here, we used 2.42 eV for an excitation wavelength of 514 nm [59].

**Table 4.1** The results from Raman spectroscopy: nanographite

Sample	Raw Graphite	Nanographite
G-band intensity	99061.6	115006
G-band position	$1581\text{ cm}^{-1}$	$1577\text{ cm}^{-1}$
D-band intensity	8353.94	57806.7
D-band position	$1354\text{ cm}^{-1}$	$1350\text{ cm}^{-1}$
$I_D/I_G$	0.0843	0.5026
$L_a$	193.69 nm	32.49 nm

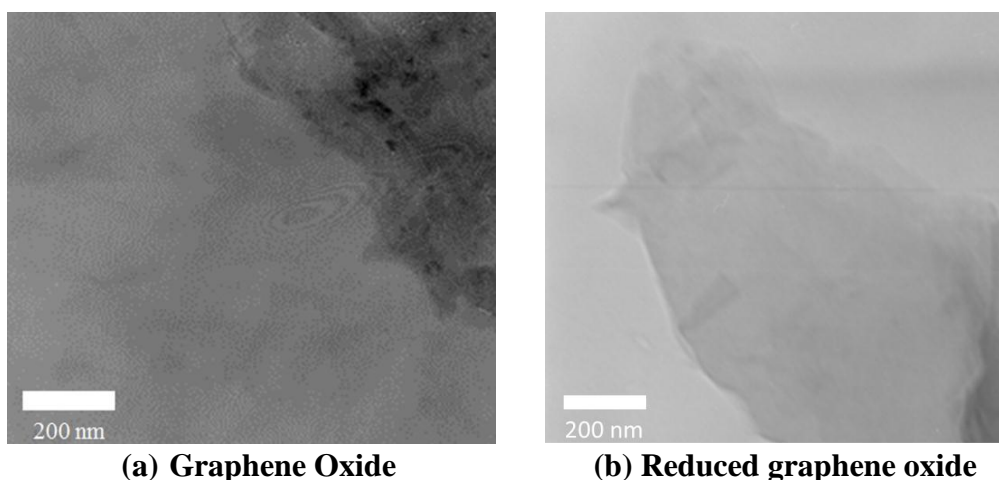
## 4.2 Reduced Graphene oxide

Figure 4.7 showed photos of graphene oxide and reduced graphene oxide suspension. It demonstrated the color changes in graphene oxide before and after reduction. The change in color from yellow brown to black can be occurred due to the effect of reduction. The reduction in a colloid state by hydrazine reduction, usually results in a black precipitation from the original yellow brown suspension, which is probably a result of an increase in the hydrophobicity of graphene oxide sheets caused by the elimination of oxide functional group out of graphene oxide sheets or a decrease in polar functionality on the surface of graphene oxide sheets. This is in a good agreement with the literature [60].



**Figure 4.7** Photos of (a) graphene oxide and (b) reduced graphene oxide suspension

The morphology and structure of the graphene oxide obtained from Hummers' method were observed by TEM in figure 4.8(a). This result indicated that we obtained graphene oxide after treating graphite with strong oxidizers. Dispersion of graphite in basic solutions yielded monomolecular sheets or graphene oxide which is the single layer form of graphite oxide. There are plenty of graphene oxides stacked on the graphene oxide. The crumpled structure of the graphene oxide maybe due to the multiplicity of oxygen functionalities in thin graphene oxide layers. TEM image in figure 4.8(b) indicated that the reduced graphene oxide as well as graphene oxide has the tendency to scroll and wrinkle.



**Figure 4.8** TEM images of (a) graphene oxide and (b) reduced graphene oxide which obtained from Hummers' method

Figure 4.9 showed Raman spectra of raw graphite and reduced graphene oxide which contains both G and D bands at  $1590$  and  $1351$   $\text{cm}^{-1}$  respectively. The G-band is from the stretching vibration of any pair of  $\text{sp}^2$  sites, whether in C=C chains. The D-band is the breathing mode of those  $\text{sp}^2$  sites only in rings, not in chains. This result indicated that the reduction started from the edges of graphene oxide particles and proceeded into the basal planes. During the reduction, parts of the basal planes near the edges became

reduced and subsequently snapped together due to  $\pi$ - $\pi$  interactions, thus narrowed the interlayer distance [61].

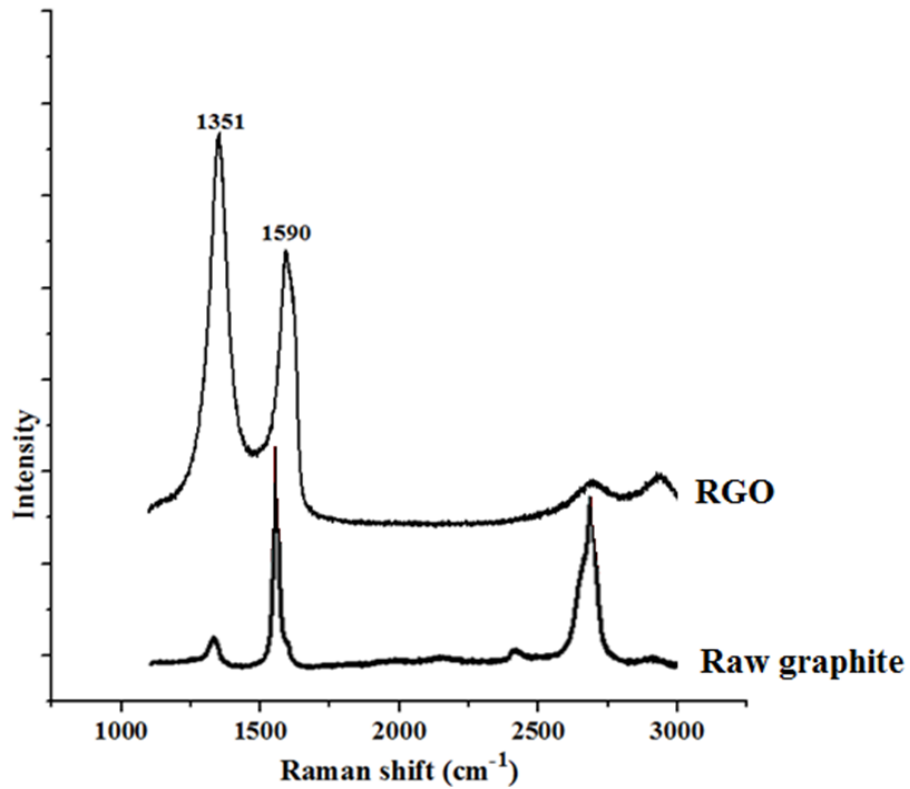


**Figure 4.9** Raman spectra of raw graphite and reduced graphene oxide (RGO)

The crystallite size of reduced graphene oxide that may attribute to the plane size of reduced graphene oxide was about 11.76 nm, which was obtained by Raman experiment using calculating by Eq. (4.1) [59].

$$L_a(\text{nm}) = \frac{560}{E_1^4} \left( \frac{I_D}{I_G} \right)^{-1} \quad (4.1)$$

where  $I_D/I_G$  is the intensity ratio of the D and G bands.  $E_1$  is the excitation laser energy in eV units. Here, we use 2.42 eV for an excitation wavelength of 514 nm [59].

**Table 4.2** The results from Raman spectroscopy: reduced graphene oxide

Sample	Raw Graphite	Reduced graphene oxide
G-band intensity	99061.6	6306
G-band position	1581 $\text{cm}^{-1}$	1590 $\text{cm}^{-1}$
D-band intensity	8353.94	8754
D-band position	1354 $\text{cm}^{-1}$	1351 $\text{cm}^{-1}$
$I_D/I_G$	0.0843	1.3882
$L_a$	193.69 nm	11.76

### 4.3 Nanographite-based pH sensor (device A)

Figure 4.10 showed SEM images of nanographite deposited in between the 1 mm electrode gap, which was obtained from 72 hour of sonication. The inset represented higher magnification image. Thin film made from self-assembly of such nanographite sheets was prepared from drop-casting technique.

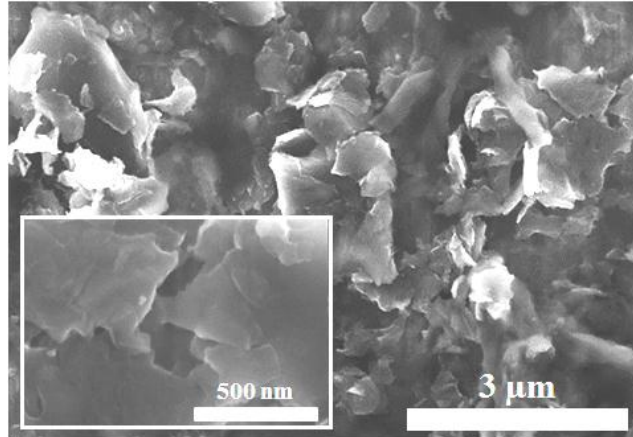


**Figure 4.10** SEM image of assembly of nanographite flakes as a film

The resistances were measured using digital multimeter. The nanographite-based pH sensor (device A) changed the resistance values upon doping with liquids of different pH are illustrated by table 4.3 and figure 4.11.

**Table 4.3** The average resistance values changing of nanographite sensor upon doping with liquids of different pH values

Sample	Without nanographite (MΩ)	With nanographite (MΩ)
pH 1	14.70	3.98
pH 2	16.89	3.66
pH3	14.36	3.59
pH 4	18.45	3.24
pH 5	16.76	3.00
pH 6	15.37	2.82
pH 7	12.34	2.35
pH 8	11.02	2.08
pH 9	11.34	1.83
pH 10	11.12	1.47
pH 11	10.09	1.40
pH 12	10.21	1.34
pH 13	10.11	1.21
pH 14	9.65	1.14

When a drop of liquid (2  $\mu\text{L}$ ) with pH 1 was placed in between gold electrodes (without nanographite) the resistance equals about 14.70  $\text{M}\Omega$ . However, at the same pH condition, but with the nanographite film deposited between the electrodes, the resistance was decreased to 3.98  $\text{M}\Omega$ .

When liquid with pH 14 was placed between gold electrodes (without nanographite), the resistance is about 9.65  $\text{M}\Omega$ . However, the resistance was decreased to 1.14  $\text{M}\Omega$  when liquid with pH 14 was placed on one with nanographite film. It should be noted that each resistance value was averaged from 20 times of measurement.

Figure 4.11 showed the comparison of resistance data of nanographite-based pH sensor which plotted against pH values, including with and without nanographite. This result demonstrated that the curve of nanographite-based pH sensor with nanographite can be described by a linear correlation which  $R^2$  is 0.97 because its resistance changes upon doping with liquids of different pH, demonstrating a linear resistance-pH relationship. For pH sensor without nanographite, the trend of its resistance did not clear because its curve was fluctuated. Therefore, pH sensor with nanographite was better than one without nanographite.

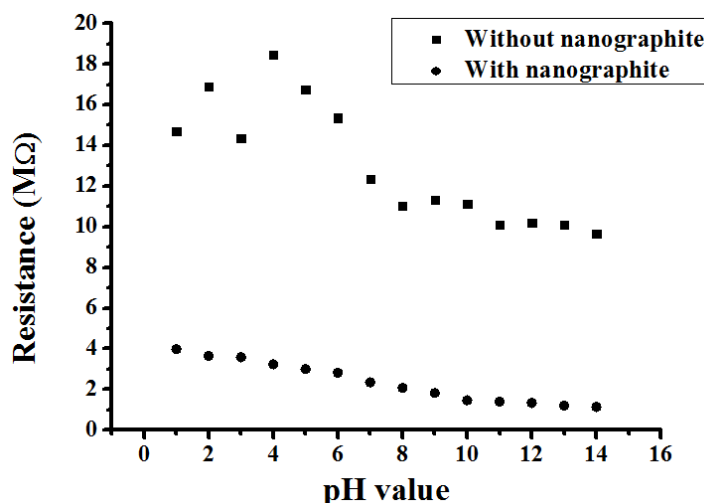


**Figure 4.11** Resistance data plotted against pH values of nanographite-based pH sensor, including with and without nanographite

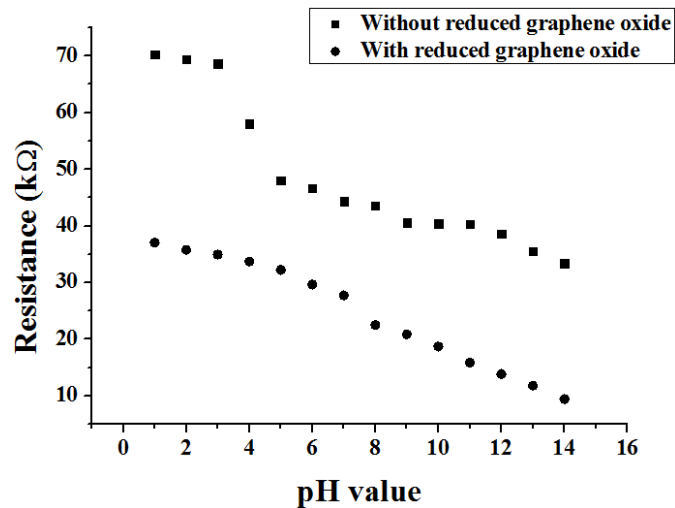
#### 4.4 Reduced graphene oxide-based pH sensor (device B)

Table 4.4 showed that the reduced graphene oxide-based pH sensor (device B) changed the resistance values upon doping with liquids of different pH.

When a drop of liquid (4  $\mu\text{L}$ ) with pH 1 and pH 14 were placed on gold electrodes (without reduced graphene oxide) the resistance equaled to 70.31 and 33.42  $\text{k}\Omega$ , respectively. However, at the same pH condition, but with the reduced graphene oxide film deposited on the electrodes, the resistance was decreased to 37.06 and 9.44  $\text{k}\Omega$  for pH 1 and 14 respectively. It should be noted that each resistance value was averaged from 20 times of measurement.

**Table 4.4** The average resistance values changing of reduced graphene oxide sensor upon doping with liquids of different pH values

Sample	Without reduced graphene oxide (k $\Omega$ )	With reduced graphene oxide (k $\Omega$ )
pH 1	70.31	37.06
pH 2	69.46	35.77
pH 3	68.65	34.93
pH 4	58.01	33.70
pH 5	47.98	32.23
pH 6	46.71	29.65
pH 7	44.32	27.73
pH 8	43.61	22.51
pH 9	40.59	20.86
pH 10	40.45	18.70
pH 11	40.32	15.88
pH 12	38.57	13.84
pH 13	35.54	11.79
pH 14	33.42	9.44



**Figure 4.12** Resistance data plotted against pH values of reduced graphene oxide-based pH sensor, including with and without reduced graphene oxide

Figure 4.12 showed the comparison of resistance data of reduced graphene oxide-based pH sensor which plotted against pH values, including with and without reduced graphene oxide. This result demonstrated that the curve of reduced graphene oxide-based pH sensor with reduced graphene oxide can be described by a linear correlation which  $R^2$  is 0.98 because its resistance changes upon doping with liquids of different pH, demonstrating a linear resistance-pH relationship. For pH sensor without reduced graphene oxide, the trend of the resistance was not a linear relationship with pH values. pH sensor with reduced graphene oxide was better than reduced one without reduced

graphene oxide, because the detection of pH sensor with reduced graphene oxide was clearer and stable than the pH sensor without reduced graphene oxide.

#### 4.5 The sensing mechanism of nanographite and reduced graphene oxide-based pH sensor

The sensing mechanism of nanographite and reduced graphene oxide (device A and B respectively) can be explained by the hydroxonium ions ( $\text{H}_3\text{O}^+$ ) and hydroxyl ions ( $\text{OH}^-$ ) adsorbed on surface of nanographite and reduced graphene oxide in the inner Helmholtz plane as shown in figure 4.13. The absorbed ions in an acid and a base are  $\text{H}_3\text{O}^+$  and  $\text{OH}^-$ , respectively. Both ion adsorption mechanisms are nonfaradaic or capacitive in which the charges cannot transmit across nanographite and reduced graphene oxide. The ability of charge storing of nanographite and reduced graphene oxide surface caused the reduction of the resistance as the follow [3].

$$i_c = C \frac{dV}{dt} \quad (4.2)$$

$$R = \frac{V}{I} \quad (4.3)$$

where  $i_c$  is the current of capacitor,  $C$  is capacitance (F),  $V_c$  is the voltage of capacitor,  $R$  is resistance ( $\Omega$ ),  $V$  is voltage (V) and  $I$  is current (A).

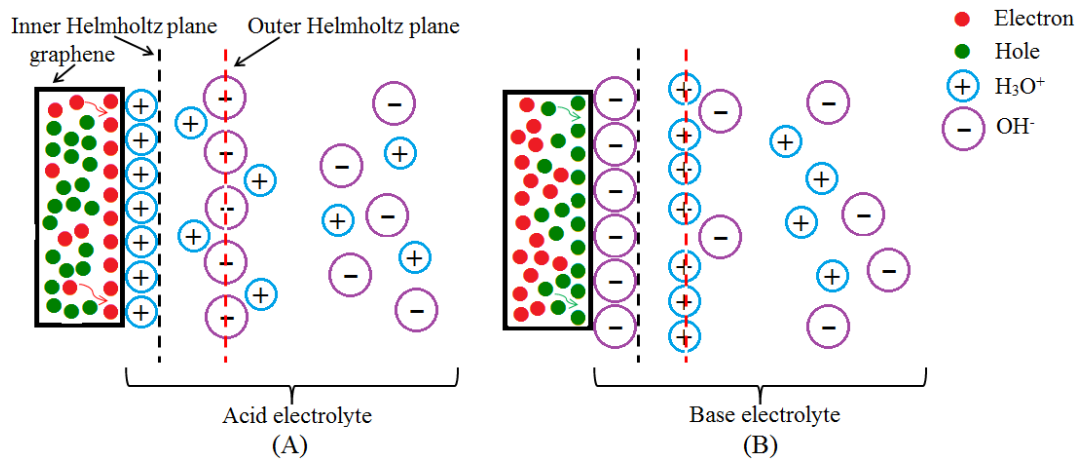


**Figure 4.13** Helmholtz plane [3]

The n-doping and p-doping of nanographite and reduced graphene oxide make by hydroxonium ions ( $\text{H}_3\text{O}^+$ ) and hydroxyl ions ( $\text{OH}^-$ ), respectively. The arrangement of hydroxyl ions ( $\text{OH}^-$ ) in the inner Helmholtz region is more ordered than hydroxonium ions ( $\text{H}_3\text{O}^+$ ) [3]. Therefore, the resistances of the sensor decrease with increasing pH values in the range of 1-14 as shown in table 4.3 and 4.4.

Figure 4.14(a) and (b) showed the average values (dots) and standard deviations (error bars) of the resistance of the nanographite and reduced graphene oxide-based pH sensor which changes upon doping with liquids of different pH respectively. The curve of device A in figure 4.12(a) was described by a linear correlation, followed by  $R = (-0.22$

$\times \text{pH} + 3.97) \text{ M}\Omega$ . This equation signified that the sensitivity of the particular sensor is  $220 \text{ k}\Omega \text{ pH}^{-1}$ . A linear equation of device B is  $R = (-2.30 \times \text{pH} + 41.97) \text{ k}\Omega$  which sensitivity is  $2.30 \text{ k}\Omega \text{ pH}^{-1}$ . These results indicate that device A is more sensitive in the detection than device B.

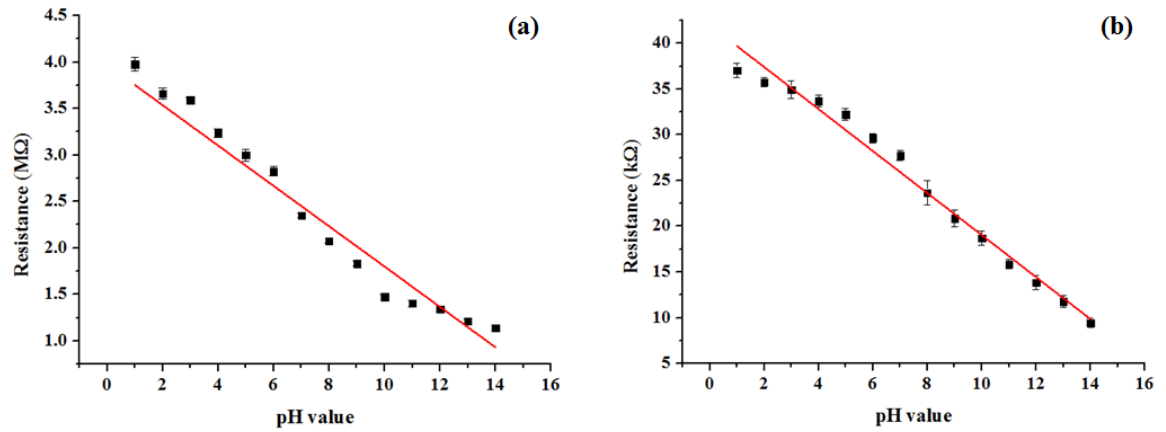


**Figure 4.14** Resistance data plotted against pH values (a) nanographite (device A) (b) reduced graphene oxide (device B)

$$\Delta\text{pH} = \frac{\sigma_{\max}}{k} \quad (4.4)$$

The standard deviation can be used to estimate the pH resolution as in Eq. (4.4). Where  $\Delta\text{pH}$  is the resolution of nanographite and reduced graphene oxide pH sensor,  $\sigma_{\max}$  is the maximum standard deviation of resistance for measurement from pH 1 to 14 and  $k$  is the sensitivity of a particular device. The standard deviation ( $\sigma$ ) at each pH value is shown in table 4.5.

**Table 4.5** Standard deviations of the sensor from pH 1 to 14

pH value	$\sigma$ of device A ( $\text{M}\Omega$ )	$\sigma$ of device B ( $\text{k}\Omega$ )
1	0.071	0.771
2	0.062	0.534
3	0.028	0.974
4	0.043	0.648
5	0.064	0.651
6	0.049	0.502
7	0.026	0.539
8	0.024	0.897
9	0.024	0.949
10	0.029	0.806
11	0.036	0.497
12	0.026	0.787
13	0.023	0.654
14	0.029	0.533

In an acid of device A,  $\sigma_{\max}$  is  $0.071 \text{ M}\Omega$ , and in a base,  $\sigma_{\max}$  is  $0.036 \text{ M}\Omega$ . The pH resolution is calculated by Eq. (4.4). We can get the pH resolution of 0.32 and 0.16 pH in acid and base, respectively. For device B,  $\sigma_{\max}$  in acid is  $0.974 \text{ k}\Omega$ , and in a base,  $\sigma_{\max}$  is  $0.949 \text{ k}\Omega$ . The pH resolution is 0.42 and 0.41 pH in acid and base, respectively. These results indicate that a change of pH resolution is reflected in the sensing mechanism when pH changes from acid to base which caused the arrangement in the inner Helmholtz region is more ordered. This is in a good agreement with the literature [3].

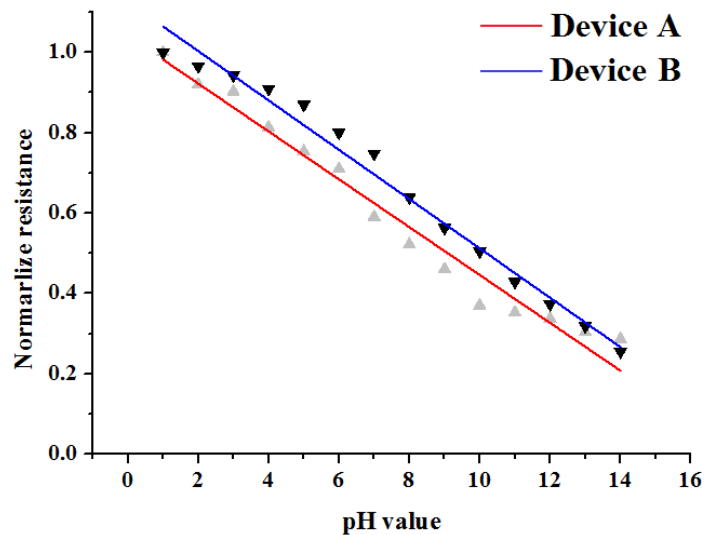


**Figure 4.15** Normalized resistances versus pH values for device A and B

To studies the difference of device A and B, we were plot the normalized resistances versus pH values. These results indicate that the sensing trend of device A and B is same. They confirm that both of devices can be used as pH sensor which resistance changes upon doping with liquids of different pH.